Crystal-Face-Dependent Charge Dynamics on a BiVO4 Photocatalyst Revealed by Single-Particle Spectroelectrochemistry

Tachikawa, Takashi

Ochi, Tomoya

Kobori, Yasuhiro

(Citation)
ACS Catalysis,6(4):2250-2256

(Issue Date)
2016-04

(Resource Type)
journal article

(Version)
Accepted Manuscript

Crystal-Face-Dependent Charge Dynamics on a $BiVO_4$ Photocatalyst Revealed by Single-Particle Spectroelectrochemistry

Takashi Tachikawa,[†,‡,*] *Tomoya Ochi,*[†] *and Yasuhiro Kobori*[†]

† Department of Chemistry, Graduate School of Science, Kobe University, 1-1 Rokkodai-cho, Nada-ku, Kobe 657-8501, Japan

‡ PRESTO, Japan Science and Technology Agency (JST), 4-1-8 Honcho Kawaguchi, Saitama 332-0012, Japan

AUTHOR INFORMATION

Corresponding Author

tachikawa@port.kobe-u.ac.jp.

ABSTRACT. The performance of semiconductor materials in solar water splitting and other applications is strongly influenced by the structure-related dynamics of charge carriers in these materials. In this study, we assessed the trapping, recombination, and surface reactions of photogenerated and electrically-injected charges on specific facets of the promising visible active photocatalyst $BiVO_4$ by using single-particle photoluminescence (PL) spectroscopy. Evaluation of the electric potential-induced PL properties and the PL response to charge scavengers revealed that the visible PL bands observed during visible laser irradiation originate from radiative recombination between holes trapped at the intraband states above the valence band and mobile (free or shallowly trapped) electrons. Furthermore, the trapped holes are preferentially located on the lateral {110} facets of the $BiVO_4$ crystal, while the electrons are uniformly distributed over the crystal. The methodology described in this study thus provides us with a unique opportunity to explore whether or not the crystal faces affect the charge carrier dynamics in the photocatalysis and the photoelectrocatalysis.

KEYWORDS: Bismuth vanadate, Electrochemistry, Interfacial charge transfer, Photocatalysis, Photoluminescence, Single-particle spectroscopy, Surface reaction

Semiconductor-based solid photocatalysts have been extensively investigated and developed for use in the production of clean and renewable chemical fuels from water or carbon dioxide, the degradation of organic/inorganic pollutants, etc.[1-3] In general, the performance of such photocatalysts is not only governed by the bulk composition but also largely by the physicochemical properties of the respective surfaces possessing different atomic arrangements and coordination. It is thus anticipated that the efficiency and selectivity of photocatalytic chemical reactions can be controlled by exposing specific facets of the crystals with controlled morphology.[4,5]

The question of whether certain crystal facets favor reduction or oxidation has been evaluated for the design of efficient photocatalysts. In 2002, Ohno et al. demonstrated that Pt particles are deposited via the photoreduction of Pt^{4+} only on the {101} facets of anatase TiO_2, whereas PbO_2 particles were formed by photooxidation of Pb^{2+} mostly on the {001} facets.[6,7] From these studies, it can be inferred that the {101} and {001} facets respectively act as preferable reduction and oxidation sites. The crystal-face dependency is proposed to be derived from the difference in the potential energy levels of the conduction band (CB) and valence band (VB) of the two facets, leading to spatial separation of the electrons (e^-) and holes (h^+) in a crystal. Recently, Li and co-workers found that the photo-deposition of reduction and oxidation cocatalysts respectively took place selectively on the {010} and {110} facets of $BiVO_4$ crystals.[8] They attributed this phenomenon to a slight difference in the energies of the CB and VB of the {010} and {110} facets, which was supported by density functional theory (DFT) calculations. In addition to the aforementioned studies, several groups have reported outcomes that are indicative of crystal-face-dependent photocatalysis on Cu_2O,[9] α-Fe_2O_3,[10] Ag_3PO_4,[11] and BiOCl.[12]

Despite significant efforts to develop solid photocatalysts with specific shapes, the crystal face effects remain poorly understood. One of the potential difficulties in investigating this complex problem is the identification and characterization of the chemical reactions taking place on the crystal surfaces under various operating conditions. In-situ microscopic observation is a very powerful tool for exploring the structural and kinetic features of (photo)catalysis, which are always hidden in the ensemble average; the advantages of in-situ microscopy are derived from the high sensitivity, selectivity, and spatial resolution.[13-17] For instance, using aqueous-phase atomic force microscopy (AFM), Mul et al. found that the photo-deposition of Pt nanoparticles on platelike WO_3 crystals takes place preferentially on the specific facets with intrinsic surface charges rather than those with photogenerated charges.[18] Tachikawa et al. studied the spatial distribution of the photocatalytic sites on anatase TiO_2 crystals using a wide-field microscope and redox-responsive fluorogenic probes.[19,20] They discovered that the reduction reaction proceeds on the lateral {101} facets of the crystal, whereas oxidation occurs primarily on the {001} planes, which is generally consistent with the above-mentioned results obtained by the selective metal deposition method. Very recently, Zhu et al. revealed that the surface photovoltage signal intensity on the {011} facet of $BiVO_4$ was 70 times stronger than that on the {010} facets, which is caused by anisotropic photoinduced charge transfer between different facets of a single crystal.[21] However, the underlying fundamental issues, including face-specific charge migration and trapping, have not been satisfactorily resolved under actual operating conditions. Such information would provide an avenue for rational design of new and more efficient photocatalysts with controlled morphology and preferentially exposed facets, such as TiO_2 mesocrystals and their composites with functional nanomaterials.[22-26]

Herein, we provide experimental evidence of the crystal-face dependence of the charge carrier dynamics on $BiVO_4$, along with a detailed analysis of the mechanisms. Monoclinic scheelite $BiVO_4$ has attracted particular interest as a promising photoanode material for solar water splitting because its band gap of 2.4–2.5 eV (absorption edge: 500–520 nm) and valence band edge of ca. 2.5 V vs. the reversible hydrogen electrode (RHE) provide a strong driving force for water oxidation by photogenerated h^+ under visible-light irradiation.[27-29] Spatially and temporally resolved photoluminescence (PL) spectroelectrochemistry[30-34] was utilized to explore the nature and spatial distribution of the trap states inherent in individual $BiVO_4$ crystals for the first time (Figure 1a). The PL emission from semiconductors is a particularly useful probe for crystal structure, particle size, and defect state evaluation because the peak positions in the spectrum and the lifetimes are strongly dependent on these structural characteristics.[35,36] These microscopic techniques thus enable us to ascertain the location of the luminescent active sites that are related to the trapping probability of the photo- and electrically-generated charge carriers on the specific facets, which is presumably dependent on the electronic energy levels of the facets and heterogeneous distribution of the effective trapping sites.

The as-synthesized $BiVO_4$ microcrystals with truncated tetragonal bipyramid morphology (see Figure 1a and the scanning electron microscope (SEM) image in Figure S1) have a monoclinic scheelite structure that can be verified from their powder X-ray diffraction (XRD) pattern and UV-visible diffuse reflectance spectrum (Figure S2 and S3). Figure 1b presents an example of single-particle PL measurements of a $BiVO_4$ crystal deposited on an indium tin oxide (ITO)-coated cover glass during photoirradiation with a continuous wave (CW) 405 nm laser. The PL intensity is inhomogeneous over the crystal, suggesting heterogeneous spatial distribution of the emissive sites. The visible emission from $BiVO_4$ is assigned to the radiative recombination of e^-

and h^+ trapped at the crystalline defects (*Vide infra*). As shown in Figure 1c (black line), the broad PL emission from the target sample is a superposition of narrower peaks and has a maximum at around 670 nm (ca. 1.85 eV), which is intermediate between the values reported by Long et al. (600 nm at room temperature)[37] and Sasaki et al. (715 nm at 25 K).[38] Furthermore, the spectral features obtained at the same location of the crystal are not dependent on the excitation wavelengths (405 and 488 nm) used to excite the e^- from the VB to the CB. Recent DFT calculations and X-ray spectroscopy have shown that the upper part of the VB is dominated by O 2p states with a small contribution from the Bi 6p and V 3d states, and the lower part of the CB is composed primarily of electronic states associated with V 3d.[39,40] Therefore, it can be deduced that the photogenerated h^+ effectively migrate and are trapped at the trap sites located above the VB under visible light irradiation ($\lambda > 400$ nm) (Figure S4).

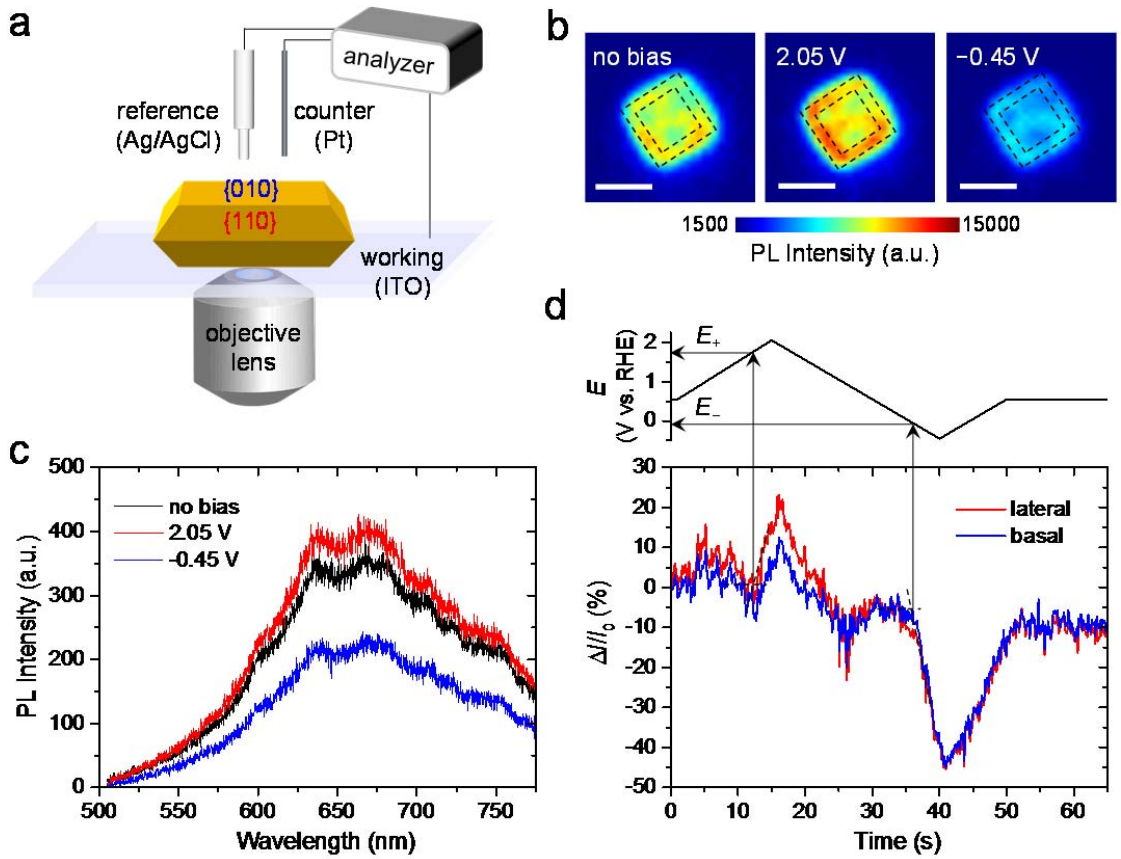

Figure 1. (a) Illustration of the sample and experimental setup for single-particle spectroelectrochemistry. (b) PL images of a single $BiVO_4$ crystal on the ITO substrate in aqueous solution of Na_2SO_4 (0.2 M, pH 6.0) under 405 nm laser irradiation without an applied potential and with applied potentials of +2.05 and −0.45 V vs. RHE. The PL intensity was integrated over all wavelengths. Scale bars are 1 μm. (c) Applied potential dependence of the PL spectra of the same $BiVO_4$ crystal under 405 nm laser irradiation. (d) Applied potential dependence of the PL intensity changes obtained for the different locations of a $BiVO_4$ crystal. *I* is the integrated intensity over all wavelengths. The black lines and arrows indicate the potential at which PL ($E_{+/-}$) is enhanced or quenched.

Single-particle spectroelectrochemistry was utilized to explore the nature of the luminescent defects present in single $BiVO_4$ crystals (Figure 1a). In a typical cyclic voltammetry (CV)

experiment, the potential of the working electrode (i.e., ITO) was linearly scanned at a scan rate of 0.1 Vs^{-1} with simultaneous measurement of the PL images or spectra of single particles.

Figure 1b shows typical PL images of a single $BiVO_4$ crystal acquired without an applied potential (E) and with E of +2.05 and −0.45 V vs. RHE. An applied voltage of +2.05 V caused a small increase in the PL intensity, whereas significant PL quenching (ca. 40%) was observed upon application of E = −0.45 V. Similar responses were observed under 488 nm laser irradiation, whereas no PL at all was detected in the absence of laser irradiation. Figure 1d further illustrates the potential dependence of the PL intensity, captured at the crystal edge and center positions (see squares enclosed by broken lines in Figure 1b), which correspond to lateral {110} and basal {010} facets, respectively. The position and morphology of the $BiVO_4$ crystals were determined from the optical transmission and SEM images,[19] and the facets were indexed from transmission electron microscope (TEM) images and selected area electron diffraction (SAED) patterns (Figure S5). The intensity trajectories seem to follow the potential cycle with specific time lags and exhibit two peaks of opposite sign at extreme potentials of +2.05 and −0.45 V vs. RHE. Interestingly, as shown in Figure 1d, the PL enhancement is more pronounced on the lateral {110} facets of the crystal at an applied voltage of >1.7 V vs. RHE. A similar tendency was observed for other crystals (Figure S6). From these results, it can be inferred that the lateral {110} facets are preferentially oxidized relative to the basal {010} facets. We further confirmed a superior oxidation ability of the {110} facets using a fluorescence dye probe, 3'-*p*-hydroxyphenyl fluorescein (HPF), as demonstrated in the Supporting Information (Figure S7).[24] The facet-dependence observed here is qualitatively consistent with the results of selective photo-deposition of metal ions,[8] spatially-resolved surface photovoltage spectroscopy,[21] and

DFT calculations.[41] On the other hand, almost uniform PL quenching over the entire crystal was induced by potentials of less than −0.1 V vs. RHE.

Here, we introduce two parameters, i.e., $E_{+/-}$ and $\Delta I/I_0$ where E and I denote the applied potential and the PL intensity, respectively to explore the responsivity of ΔI (= $I - I_0$) to $E_{+/-}$ and the spatial uniformity of the responses. The potentials at which enhancement and quenching of the PL were initiated are defined as E_+ and E_-, respectively, and were determined for individual crystals. As seen in Figure 2a, the histograms of E_+ for the basal and lateral facets indicate broad distributions with peaks at +1.71 (± 0.01) and +1.62 (± 0.02) V vs. RHE, respectively. The difference (ca. 0.1 eV) of the mean E_+ values is about 4 times larger than the thermal energy (0.025 eV) at room temperature and is considerably smaller than the difference (0.42 eV) of the VB edge between the two facets, which was obtained by DFT calculations.[8] In contrast, the mean E_- values (0.00 (± 0.01) V vs. RHE) determined from both facets were almost the same (Figure 2b).

A more striking difference was seen in the PL intensity changes using an applied voltage of +2.05 V vs. RHE ($\Delta I_+/I_0$). As shown in Figure 2c, the mean $\Delta I_+/I_0$ value of the lateral facets is nearly 2 times on average larger than that of the basal facets, whereas the mean $\Delta I_-/I_0$ values were almost identical for both facets at E = −0.45 V vs. RHE (Figure S8). This result supports the previous observation that the effective h^+ trapping sites are preferentially located on the {110} facets. The intensity of the spectral peaks increased or decreased during the potential cycle without any change in the spectral features (red and blue lines in Figure 1c), implying that identical trap sites are involved in the potential-induced PL process.

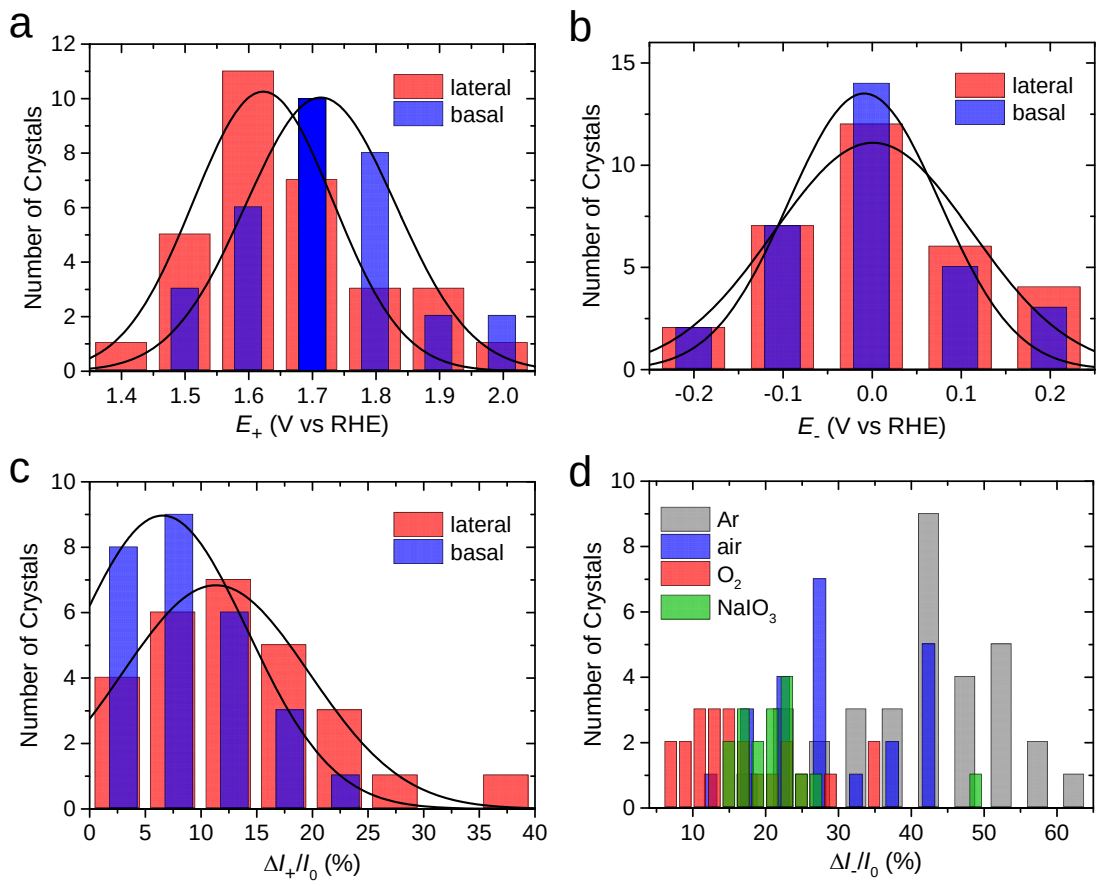

Figure 2. (a,b) Histograms of E_+ (a) and E_- (b) determined for individual $BiVO_4$ crystals. The number of the analyzed crystals is 31. The black lines indicate the Gaussian distribution fitted to the histograms. Corrected R^2 are 0.81 and 0.93 for E_+ and 0.88 and 0.89 for E_- on the lateral and basal facets, respectively. (c) Histograms of $\Delta I_+/I_0$ determined for individual $BiVO_4$ crystals. ΔI_+ is obtained from $I_+ - I_0$, where I_+ is the PL intensity at E = +2.05 V vs. RHE and I_0 is the PL intensity without potential. The number of the analyzed crystals is 27. The black lines indicate the Gaussian distribution fitted to the histograms. The maxima were determined to be 11.3 (± 0.5) and 6.5 (± 0.4) % for the lateral and basal facets, respectively. Corrected R^2 are 0.97 and 0.99 for $\Delta I_+/I_0$ on the lateral and basal facets, respectively. (d) Histograms of $\Delta I_-/I_0$ determined for individual $BiVO_4$ crystals in the absence or presence of electron scavengers. The I_- values were obtained at E = −0.45 V vs. RHE.

The CB edge of $BiVO_4$ (E_{CB}) was ca. −0.05 V vs. RHE, as calculated from the reported flat-band potential (−0.6 ± 0.1 V vs. Ag/AgCl at pH 5.8).[42] From this evaluation, it can be deduced that the potential application of −0.45 V vs. RHE leads to the accumulation of e^- in the CB of $BiVO_4$. From the E_{CB} and the bandgap of $BiVO_4$ (2.34 eV, Figure S3), the VB edge (E_{VB}) was readily calculated as +2.29 V vs. RHE. The determined mean E_+ value of ca. +1.7 V vs. RHE (= +1.3 V vs. NHE or +1.1 V vs. Ag/AgCl) thus indicates that the photogenerated h^+ are trapped at intraband states with energies of ca. 0.7 eV above the E_{VB}. Considering the PL peak energy of ca. 1.8 eV (λ = 670–690 nm), it can be deduced that trapped h^+ recombine free or shallowly-trapped e^-.

The PL quenching induced by an applied negative potential was also evaluated. As demonstrated in Figure 2b, the average E_- value was determined to be ca. 0 V vs. RHE (= −0.35 V vs. NHE or −0.55 V vs. Ag/AgCl), which is comparable with the CB edge of ca. −0.05 V vs. RHE, again supporting the assignment of the PL spectra. To clarify the origin of the PL quenching, electron scavengers such as oxygen (1.3 mM) and $NaIO_3$ (50 mM) were added to the electrolyte solutions and the PL responses of individual crystals were monitored during the potential cycle. As shown in Figure 2d, PL quenching was significantly suppressed in the presence of electron scavengers, while the scavengers had no significant effect on the PL enhancement induced by positive potential (Figures S9 and S10). These results are reasonable because the E_{CB} is more negative than the reduction potential of molecular oxygen (−0.33 V vs. NHE, $O_2 + e^- \rightarrow O_2^-$)[43] and that of IO_3^- (0.67 V vs. NHE, $4H^+ + (2/3)IO_3^- + 4e^- \rightarrow (2/3)I^- + 2H_2O$) in aqueous solution.[44] An alternative path for consumption of the e^-, involving molecular oxygen, was proposed as follows: $O_2 + H^+ + e^- \rightarrow {}^{\bullet}O_2H$.[45] IO_3^- should act as a better electron scavenger due to its larger driving force and higher concentration than O_2, but the result in

Figure 2b is contrary to this expectation. The isoelectric point of $BiVO_4$ was reported as 4.56[46] and a zeta potential of $BiVO_4$ aqueous dispersion was −31.4 mV at pH = 6,[47] thus suggesting that the adsorption of IO_3^- is partially inhibited due to the negatively charged surface of $BiVO_4$.

Furthermore, slow PL decay was observed after discontinuing application of the pulsed negative potential (Figure 3a). The PL decay time decreased from 2.1 s to 0.86 s, as determined from single-exponential fitting, upon altering the environment from an Ar-saturated solution to an O_2-saturated ($[O_2]$ = 1.4 mM) solution; this strongly supports our conclusion that mobile (or trapped) e^- are captured by oxygen molecules in the electrolyte solution. Transient visible-NIR-IR absorption measurements previously revealed that free electrons in TiO_2 react with molecular oxygen in air-saturated methanol ($[O_2]$ = 2.1 mM) within microseconds to milliseconds.[48] This result is reasonable in light of the fact that a carrier mobility of $BiVO_4$ (0.044 $cm^2\ V^{-1}\ s^{-1}$) is lower by a few orders of magnitude than those of typical metal oxides (e.g., TiO_2, WO_3, Cu_2O).[49] The much slower electron transfer on $BiVO_4$ is also probably due to its lower CB potential compared with that of TiO_2 (E_{CB} = −0.58 V vs. NHE at pH 7).[50] Because of the poor reduction ability of $BiVO_4$, addition of sacrificial electron acceptors such as Ag^+ is needed for efficient photocatalytic reactions.[45,51]

Furthermore, as shown in Figure 3b, relatively short-lived PL signals with a lifetime of 0.6 ± 0.2 s were observed following application of a pulsed positive potential. Recently, water oxidation on $BiVO_4$ occurred at a rate constant of 1.3 s^{-1} based on analysis of the transient absorption decay kinetics of trapped h^+.[52] It is thus presumable that the observed PL decay in less than a second is closely related to water oxidation by excess trapped h^+.

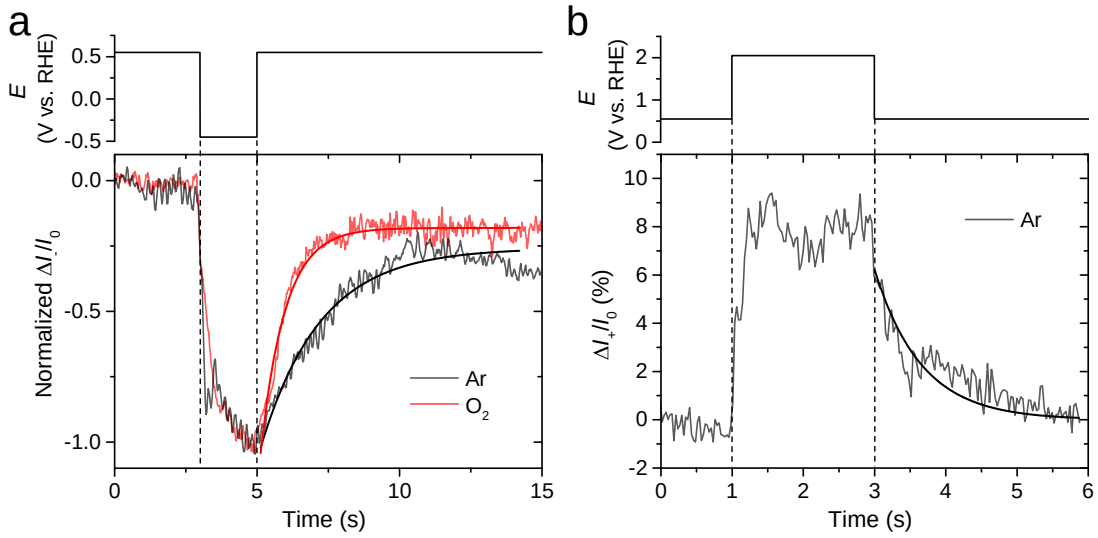

Figure 3. PL intensity changes observed for single $BiVO_4$ crystals with pulsed potentials of −0.45 (a) and +2.05 V (b) vs. RHE. The bold solid lines indicate single-exponential curves fitted to kinetic traces.

A schematic diagram illustrating the charge transfer processes is proposed in Figure 4. The h^+ trapping occurs preferentially on the lateral {110} facets of the crystal under visible irradiation, resulting in the radiative recombination with the photogenerated e^- (Figure 4a). The increase in the number of the injected trapped h^+ by the positive voltages will result in the enhancement of the PL intensity because of the increased prompt radiative recombination with the photogenerated e^-. In addition to this process, trapped h^+ are consumed to produce oxygen molecules from water with a time constant of ca. 0.6 s. In contrast, electrically-injected e^- are uniformly distributed over the crystal and recombine with trapped h^+ or react with molecular oxygen. A possible explanation for the PL quenching at the negative potentials relative to the CB edge is the filling of the CB with e^- (the so-called Burstein–Moss effect),[53,54] which is generally observable as bleaching of the ground-state absorption in the optical absorption spectrum.[55-57]

Similar PL quenching upon application of negative potentials was recently observed for TiO_2 nanoparticles.[58] However, the reflectance change at 405 nm of the $BiVO_4$-coated ITO electrode with and without a potential of −0.45 vs. RHE was within 1%, thus excluding the Burstein-Moss effect as a dominant mechanism. Another possible mechanism is related to non-radiative recombination between excess e^- and h^+. The substantial number of e^- in the CB and/or non-luminescent trapping sites enhance non-radiative recombination with h^+ in the VB, which might be competitive with the h^+ trapping at the surface states, thus resulting in the PL quenching (Figure 4b). It has been suggested that the accumulated e^- in the CB increases the charge recombination rate, thus decreasing the efficiency of the water oxidation reaction.[59] Since $BiVO_4$ is an indirect semiconductor, the band-to-band recombination should be non-radiative in terms of energy and momentum conservation.[60]

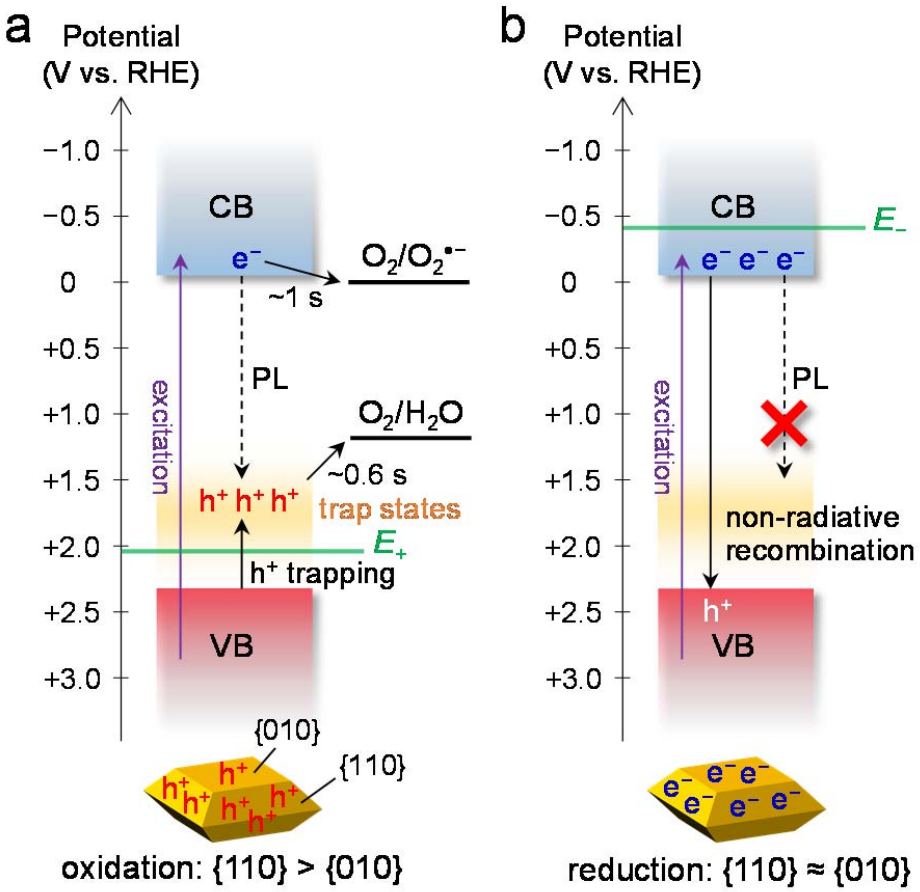

Figure 4. Schematic diagram showing the energy band structure of $BiVO_4$ and related charge transfer processes under positive (a) and negative (b) potentials.

In conclusion, we have investigated the reaction dynamics of the photo- and electrically-generated charges on the specific crystal facets of $BiVO_4$ by analysis of the PL emission from individual crystals. Potential-induced PL imaging allowed us to assess the spatial distribution and kinetics of excess charges that are responsible for solar water splitting. The specially and temporary resolved single-particle spectroelectrochemical technique should function as a complementary tool for characterizing semiconductor solid photocatalysts and studying the underlying mechanisms of (photo)catalytic reactions under various operating conditions.

EXPERIMENTAL METHODS

Synthesis of $BiVO_4$. $BiVO_4$ crystals were synthesized by a hydrothermal reaction as described elsewhere.[8] In a typical procedure, the precursors, NH_4VO_3 (36 mmol) (Wako) and $Bi(NO_3)_3 \cdot 5H_2O$ (36 mmol) (Wako), were dissolved in 300 mL of 2.0 M nitric acid solution; the pH of the solution was then adjusted to 2.0 with ammonia solution under stirring until an orange precipitate was formed. After aging for about 2 h, the orange precipitate at the bottom of the beaker was transferred to a Teflon-lined stainless steel autoclave and hydrothermally treated at 200 ^oC for 24 h. After cooling the autoclave to room temperature, a yellow powder was separated by centrifugation, washed with distilled water more than 3 times, and then dried at 60 ^oC in air.

Characterization. SEM measurements were carried out on JEOL JSM-5500 operated at 20 kV. TEM measurements were carried out on Hitach H-800 operated at 200 kV. Powder XRD measurements were carried out on Rigaku Ultima IV with Cu K_α source. Steady-state UV–visible diffuse reflectance spectra were measured using a UV–visible spectrophotometer (V-770, JASCO). All experimental data were obtained at room temperature.

Single-Particle PL Measurements. For the single-particle PL measurements, borosilicate cover glasses or ITO-coated cover glasses (100 nm thickness, 10 Ω cm^{-2}) were purchased from Matsunami Glass and cleaned by sonication in a 20% detergent solution (Cleanace, As One) for 6 h, followed by repeated washing with running water for 10 min. Finally, the cover glasses were washed with distilled water. An aqueous suspension of $BiVO_4$ was cast on the cover glass by spin coating at 2000 rpm for 50 s, followed by annealing the $BiVO_4$-coated cover glass at 90 °C for 1 h in order for the particles on the glass not to peel off during the immersion in the solution. The good physical contact between the crystals and ITO was confirmed by optical transmission and PL images. The experimental setup was based on a Nikon Ti-E inverted fluorescence

microscope. The 405-nm CW laser (OBIS 405LX, Coherent; typically 12 μW at the glass surface) was used to excite the $BiVO_4$. The emission images were recorded on an electron-multiplying charge-coupled device (EMCCD) camera (Evolve 512, Roper Scientific) at a rate of 10 or 30 frames s^{-1} using the open source microscopy software Micro-Manager (https://www.micro-manager.org/). A suitable dichroic mirror (Di02-R405, Semrock) and a longpass filter (BLP01-458R, Semrock) were used to improve the signal-to-noise ratio. All experimental data were obtained at room temperature. The data were analyzed using the open source image software ImageJ (http://rsb.info.nih.gov/ij/) and Origin 2015 (OriginLab). Single-particle electrochemical measurements were carried out using electrochemical analyzer (model 608E, ALS) with a standard three-electrode configuration. The cell configuration is illustrated in Figure 1a. The cyclic voltammetric data were collected by taking Ag/AgCl as the reference electrode at room temperature. The data can be converted to reversible hydrogen electrode (RHE) scale according to the Nernst equation ($E_{RHE} = E_{Ag/AgCl} + 0.195 + 0.059pH$).

Supporting Information. Additional results of ensemble and single-particle experiments. This material is available free of charge via the Internet at http://pubs.acs.org.

AUTHOR INFORMATION

Corresponding Author

*Email: tachikawa@port.kobe-u.ac.jp.

Notes

The authors declare no competing financial interest.

ACKNOWLEDGMENTS

This work has been partially supported by Advanced Characterization Nanotechnology Platform, Nanotechnology Platform Program of the Ministry of Education, Culture, Sports, Science and Technology (MEXT), Japan at the Research Center for Ultra-High Voltage Electron Microscopy (Nanotechnology Open Facilities) in Osaka University and a Grant-in-Aid for Scientific Research (Project 15H03771) from the MEXT, Japan.

REFERENCES

(1) Kudo, A.; Miseki, Y. *Chem. Soc. Rev.* **2009,** 38, 253-278.
(2) Chen, X.; Shen, S.; Guo, L.; Mao, S. S. *Chem. Rev.* **2010,** 110, 6503-6570.
(3) Kubacka, A.; Fernandez-Garcia, M.; Colon, G. *Chem. Rev.* **2012,** 112, 1555-1614.
(4) Liu, G.; Yang, H. G.; Pan, J.; Yang, Y. Q.; Lu, G. Q.; Cheng, H.-M. *Chem. Rev.* **2014,** 114, 9559-9612.
(5) Liu, G.; Yu, J. C.; Lu, G. Q.; Cheng, H.-M. *Chem. Commun.* **2011,** 47, 6763-6783.
(6) Ohno, T.; Sarukawa, K.; Matsumura, M. *New J. Chem.* **2002,** 26, 1167-1170.
(7) Murakami, N.; Kurihara, Y.; Tsubota, T.; Ohno, T. *J. Phys. Chem. C* **2009,** 113, 3062-3069.
(8) Li, R.; Zhang, F.; Wang, D.; Yang, J.; Li, M.; Zhu, J.; Zhou, X.; Han, H.; Li, C. *Nat. Commun.* **2013,** *4*, Article number: 1432.
(9) Zhang, Y.; Deng, B.; Zhang, T.; Gao, D.; Xu, A.-W. *J. Phys. Chem. C* **2010,** 114, 5073-5079.
(10) Yanina, S. V.; Rosso, K. M. *Science* **2008,** 320, 218-222.
(11) Martin, D. J.; Umezawa, N.; Chen, X.; Ye, J.; Tang, J. *Energy Environ. Sci.* **2013,** 6, 3380-3386.
(12) Zhang, L.; Wang, W.; Sun, S.; Jiang, D.; Gao, E. *Appl. Catal., B* **2015,** 162, 470-474.
(13) Weckhuysen, B. M. *Angew. Chem., Int. Ed.* **2009,** 48, 4910-4943.
(14) Buurmans, I. L. C.; Weckhuysen, B. M. *Nat. Chem.* **2012,** 4, 873-886.
(15) De Cremer, G.; Sels, B. F.; De Vos, D. E.; Hofkens, J.; Roeffaers, M. B. J. *Chem. Soc. Rev.* **2010,** 39, 4703-4717.
(16) Tachikawa, T.; Majima, T. *Chem. Soc. Rev.* **2010,** 39, 4802-4819.
(17) Warren, S. C.; Voitchovsky, K.; Dotan, H.; Leroy, C. M.; Cornuz, M.; Stellacci, F.; Hebert, C.; Rothschild, A.; Graetzel, M. *Nat. Mater.* **2013,** 12, 842-849.

(18) Wenderich, K.; Klaassen, A.; Siretanu, I.; Mugele, F.; Mul, G. *Angew. Chem., Int. Ed.* **2014,** 53, 12476-12479.
(19) Tachikawa, T.; Yamashita, S.; Majima, T. *J. Am. Chem. Soc.* **2011,** 133, 7197-7204.
(20) Tachikawa, T.; Majima, T. *Chem. Commun.* **2012,** 48, 3300-3302.
(21) Zhu, J.; Fan, F.; Chen, R.; An, H.; Feng, Z.; Li, C. *Angew. Chem., Int. Ed.* **2015,** 54, 9111-9114.
(22) Bian, Z.; Tachikawa, T.; Majima, T. *J. Phys. Chem. Lett.* **2012,** 3, 1422-1427.
(23) Bian, Z.; Tachikawa, T.; Zhang, P.; Fujitsuka, M.; Majima, T. *J. Am. Chem. Soc.* **2014,** 136, 458-465.
(24) Tachikawa, T.; Zhang, P.; Bian, Z.; Majima, T. *J. Mater. Chem. A* **2014,** 2, 3381-3388.
(25) Zhang, P.; Tachikawa, T.; Bian, Z.; Majima, T. *Appl. Catal., B* **2015,** 176-177, 678-686.
(26) Zhang, P.; Tachikawa, T.; Fujitsuka, M.; Majima, T. *Chem. Commun.* **2015,** 51, 7187-7190.
(27) Kudo, A.; Ueda, K.; Kato, H.; Mikami, I. *Catal. Lett.* **1998,** 53, 229-230.
(28) Kudo, A.; Omori, K.; Kato, H. *J. Am. Chem. Soc.* **1999,** 121, 11459-11467.
(29) Park, Y.; McDonald, K. J.; Choi, K.-S. *Chem. Soc. Rev.* **2013,** 42, 2321-2337.
(30) Tachikawa, T.; Ishigaki, T.; Li, J.-G.; Fujitsuka, M.; Majima, T. *Angew. Chem., Int. Ed.* **2008,** 47, 5348-5352.
(31) Tachikawa, T.; Majima, T. *J. Am. Chem. Soc.* **2009,** 131, 8485-8495.
(32) Palacios, R. E.; Fan, F.-R. F.; Grey, J. K.; Suk, J.; Bard, A. J.; Barbara, P. F. *Nat. Mater.* **2007,** 6, 680-685.
(33) Mercado, C. C.; Knorr, F. J.; McHale, J. L. *ACS Nano* **2012,** 6, 7270-7280.
(34) Galland, C.; Ghosh, Y.; Steinbrueck, A.; Sykora, M.; Hollingsworth, J. A.; Klimov, V. I.; Htoon, H. *Nature* **2011,** 479, 203-207.
(35) Nirmal, M.; Brus, L. *Acc. Chem. Res.* **1999,** 32, 407-414.
(36) Burda, C.; Chen, X.; Narayanan, R.; El-Sayed, M. A. *Chem. Rev.* **2005,** 105, 1025-1102.
(37) Long, M.; Cai, W.; Cai, J.; Zhou, B.; Chai, X.; Wu, Y. *J. Phys. Chem. B* **2006,** 110, 20211-20216.
(38) Sasaki, Y.; Nemoto, H.; Saito, K.; Kudo, A. *J. Phys. Chem. C* **2009,** 113, 17536-17542.
(39) Walsh, A.; Yan, Y.; Huda, M. N.; Al-Jassim, M. M.; Wei, S.-H. *Chem. Mater.* **2009,** 21, 547-551.
(40) Cooper, J. K.; Gul, S.; Toma, F. M.; Chen, L.; Glans, P.-A.; Guo, J.; Ager, J. W.; Yano, J.; Sharp, I. D. *Chem. Mater.* **2014,** 26, 5365-5373.
(41) Liu, T.; Zhou, X.; Dupuis, M.; Li, C. *Phys. Chem. Chem. Phys.* **2015,** 17, 23503-23510.
(42) Sayama, K.; Nomura, A.; Arai, T.; Sugita, T.; Abe, R.; Yanagida, M.; Oi, T.; Iwasaki, Y.; Abe, Y.; Sugihara, H. *J. Phys. Chem. B* **2006,** 110, 11352-11360.
(43) Ilan, Y. A.; Meisel, D.; Czapski, G. *Isr. J. Chem.* **1974,** 12, 891-895.
(44) Sayama, K.; Mukasa, K.; Abe, R.; Abe, Y.; Arakawa, H. *J. Photochem. Photobiol., A* **2002,** 148, 71-77.

(45) Saison, T.; Chemin, N.; Chaneac, C.; Durupthy, O.; Mariey, L.; Mauge, F.; Brezova, V.; Jolivet, J.-P. *J. Phys. Chem. C* **2015,** 119, 12967-12977.
(46) Wetchakun, N.; Chaiwichain, S.; Inceesungvorn, B.; Pingmuang, K.; Phanichphant, S.; Minett, A. I.; Chen, J. *ACS Appl. Mater. Interfaces* **2012,** 4, 3718-3723.
(47) Wang, Y.; Wang, W.; Mao, H.; Lu, Y.; Lu, J.; Huang, J.; Ye, Z.; Lu, B. *ACS Appl. Mater. Interfaces* **2014,** 6, 12698-12706.
(48) Yoshihara, T.; Katoh, R.; Furube, A.; Tamaki, Y.; Murai, M.; Hara, K.; Murata, S.; Arakawa, H.; Tachiya, M. *J. Phys. Chem. B* **2004,** 108, 3817-3823.
(49) Abdi, F. F.; Savenije, T. J.; May, M. M.; Dam, B.; van de Krol, R. *J. Phys. Chem. Lett.* **2013,** 4, 2752-2757.
(50) Rothenberger, G.; Fitzmaurice, D.; Grätzel, M. *J. Phys. Chem.* **1992,** 96, 5983-5986.
(51) Castillo, N. C.; Ding, L.; Heel, A.; Graule, T.; Pulgarin, C. *J. Photochem. Photobiol., A* **2010,** 216, 221-227.
(52) Ma, Y.; Pendlebury, S. R.; Reynal, A.; Le Formal, F.; Durrant, J. R. *Chem. Sci.* **2014,** 5, 2964-2973.
(53) Burstein, E. *Phys. Rev.* **1954,** 93, 632-633.
(54) Moss, T. S. *Proc. Phys. Soc., London* **1954,** 67B, 775-782.
(55) Robel, I.; Subramanian, V.; Kuno, M.; Kamat, P. V. *J. Am. Chem. Soc.* **2006,** 128, 2385-2393.
(56) Ravensbergen, J.; Abdi, F. F.; van Santen, J. H.; Frese, R. N.; Dam, B.; van de Krol, R.; Kennis, J. T. M. *J. Phys. Chem. C* **2014,** 118, 27793-27800.
(57) Boschloo, G.; Fitzmaurice, D. *J. Phys. Chem. B* **1999,** 103, 7860-7868.
(58) Rex, R. E.; Knorr, F. J.; McHale, J. L. *J. Phys. Chem. C* **2014,** 118, 16831-16841.
(59) Abdi, F. F.; van de Krol, R. *J. Phys. Chem. C* **2012,** 116, 9398-9404.
(60) Cooper, J. K.; Gul, S.; Toma, F. M.; Chen, L.; Liu, Y.-S.; Guo, J.; Ager, J. W.; Yano, J.; Sharp, I. D. *J. Phys. Chem. C* **2015,** 119, 2969-2974.

TOC GRAPHICS